

# Pump-induced Exceptional Points in Lasers

M. Liertzer,<sup>1,\*</sup> Li Ge,<sup>2</sup> A. Cerjan,<sup>3</sup> A. D. Stone,<sup>3</sup> H. E. Türeci,<sup>2,4</sup> and S. Rotter<sup>1,†</sup>

<sup>1</sup>*Institute for Theoretical Physics, Vienna University of Technology, A-1040 Vienna, Austria, EU*

<sup>2</sup>*Department of Electrical Engineering, Princeton University, Princeton, New Jersey 08544, USA*

<sup>3</sup>*Department of Applied Physics, Yale University, New Haven, Connecticut 06520, USA*

<sup>4</sup>*Institute for Quantum Electronics, ETH-Zürich, CH-8093 Zürich, Switzerland*

(Dated: February 18, 2022)

We demonstrate that the above-threshold behavior of a laser can be strongly affected by exceptional points which are induced by pumping the laser nonuniformly. At these singularities, the eigenstates of the non-Hermitian operator which describes the lasing modes coalesce. In their vicinity, the laser may turn off even when the overall pump power deposited in the system is increased. Such signatures of a pump-induced exceptional point can be experimentally probed with coupled ridge or microdisk lasers.

PACS numbers: 42.55.Sa, 42.55.Ah, 42.25.Bs

The interest in physical systems described by non-Hermitian operators has recently been revived by a number of pioneering experiments [1–7] which demonstrated the rich physics induced by the system’s non-Hermiticity. In this context exceptional points (EPs), at which non-Hermitian operators are defective and pairs of their eigenstates coalesce [8], are of particular interest. In the vicinity of these EPs the eigenvalues display an intricate topology of intersecting Riemann sheets, leading to nontrivial geometric phases when encircling the EP parametrically, as well as to problems with mode labeling [4–11].

Photonic structures in the presence of gain or loss are a natural arena in which EPs can play a role, since they are described by a non-Hermitian Maxwell operator, arising from a complex dielectric function. Striking examples which have received much attention recently are optical systems with balanced gain and loss, for which this operator is invariant under parity ( $\mathcal{P}$ ) and time-reversal ( $\mathcal{T}$ ) [12]. In such systems, as the real wave vector,  $k$ , of the input radiation is varied, the electromagnetic scattering matrix undergoes a transition at an EP from a “flux-conserving” behavior to an amplifying/attenuating behavior [13]. This transition leads to a number of novel optical properties [1, 2], such as power oscillations of light, beam steering, and self-sustained radiation [14–16].

Lasers are prototype non-Hermitian systems, with the additional complexity of being described by a nonlinear wave equation above their first oscillation threshold. Until very recently, however, no connection had been made between pumping a laser and the phenomena associated with EPs. The reason for this, as we shall see below, is that the non-Hermitian operators describing lasers do not reveal EPs when the laser is pumped *uniformly* in space. Two previous works have hinted at EP physics in non-uniformly pumped lasers. First, a work on  $\mathcal{PT}$  optical systems has shown that a cavity with balanced regions of strong gain and strong loss can actually lase *after* the  $\mathcal{PT}$ -breaking EP has been crossed [13, 17]. However, the properties of this unusual laser (which has yet to be

demonstrated experimentally) are not influenced by the EP *above* threshold. Another laser system which exhibits EPs is composed of very-low  $Q$  cavities, which can form novel surface-state lasing modes [18]. Again, however, these modes are created well away from the EP and their lasing properties are not affected by it, nor is this a practical system for experiments.

In the current Letter, we propose a class of non-uniformly pumped laser systems, which are achievable in practical laser structures and which show the dramatic role of an EP *above* the laser threshold in controlling and even switching off the coherent emission. The systems we study consist of two coherently coupled laser cavities as realized, e.g., by two coupled ridge lasers (see insets in Fig. 1). The cavities are assumed to have large loss in the absence of pumping. Their unusual behavior when pumped is shown in Fig. 1 (red curve) [19]. First the left cavity is pumped ( $0 < d < 1$ ) until it begins lasing in an asymmetric mode which emits predominantly to the left; then, pumping is added to the right cavity and increased ( $1 < d < 2$ ), which, surprisingly, causes the laser first to shut off and then to turn on again as a symmetric mode (details of the pumping scheme are given in the caption). This behavior occurs for a specific value of the center and width of the gain curve. Quite different behavior occurs if the gain center is shifted by a small amount compared to the free spectral range. If shifted down (yellow curve), the system never lases at all in the asymmetric mode; if shifted up (blue curve), it does not ever switch off, but the mode slowly evolves from asymmetric to symmetric with a strong intensity dip after the initial turn-on. We will show that this counter-intuitive dependence on the pump strength and high sensitivity to the gain curve is completely controlled by an EP in the relevant non-Hermitian operator for the laser problem.

The above results have been obtained from the stationary solutions of the nonlinear Maxwell-Bloch equations, which are the key equations in semiclassical laser theory [20, 21]. To calculate these solutions, we em-

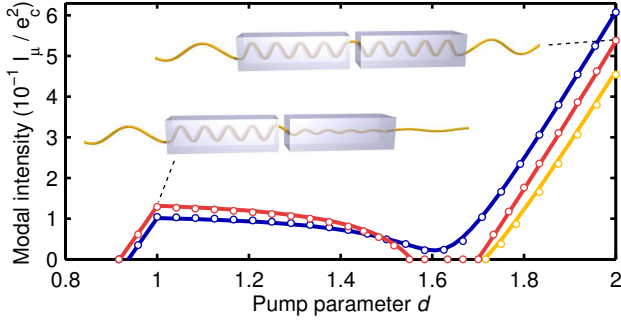


FIG. 1. (color online) Intensity output of a laser system consisting of two 1D coupled ridge lasers, each of length  $100 \mu\text{m}$  with an air gap of size  $10 \mu\text{m}$  and an (unpumped) index of refraction  $n = 3 + 0.13i$ . For  $0 < d < 1$ , the pump in the left ridge is linearly increased in the range  $0 < D < 1.2$ , and for  $1 < d < 2$ , the same is done in the right ridge while keeping the left ridge at  $D = 1.2$ . The points show the results determined from a finite-difference time-domain solution of the Maxwell-Bloch equations (using  $\gamma_{\parallel} = 0.02 \text{ mm}^{-1}$ ). The solid lines are the solutions as given by SALT (see the text). The three different colors (red, blue and yellow [19]) represent the results for different gain curves with a width of  $2\gamma_{\perp} = 4 \text{ mm}^{-1}$  centered around  $k_a = \{92.4, 94.6, 96.3\} \text{ mm}^{-1}$ , respectively. Although the overall pump power increases monotonically over the entire range of  $d$ , the laser is found to turn off in the range  $1.55 < d < 1.68$  due to the influence of an exceptional point. The insets show the electric field amplitude in the laser at the pump steps  $d = \{1, 2\}$  for the gain curve centered around  $k_a = 94.6 \text{ mm}^{-1}$ .

ployed the newly developed steady-state *ab initio* laser theory (SALT) [22–24], which is exact in the single-mode regime of interest here (except for the standard rotating wave approximation). Because of the novelty of the behavior studied here, we independently confirmed the SALT results (see lines in Fig. 1) using the more familiar finite-difference time-domain method (see points in Fig. 1) [25]. The observed reentrant behavior, however, cannot be understood in the time domain, requiring, instead, a frequency-domain approach like SALT. In 1D and 2D, the SALT equations are coupled scalar nonlinear wave equations for the lasing modes  $\Psi_{\mu}(\mathbf{x})$  and their corresponding lasing frequencies  $k_{\mu}$ , of the form [22]

$$\left[ \nabla^2 + k_{\mu}^2 \varepsilon(\mathbf{x}, \{k_{\nu}, \Psi_{\nu}\}) \right] \Psi_{\mu}(\mathbf{x}) = 0. \quad (1)$$

Here the complex dielectric function  $\varepsilon(\mathbf{x}, \{k_{\nu}, \Psi_{\nu}\}) = \varepsilon_c(\mathbf{x}) + \varepsilon_g(\mathbf{x}, \{k_{\nu}, \Psi_{\nu}\})$  comprises a contribution from the passive cavity  $\varepsilon_c$  as well as a gain contribution  $\varepsilon_g$  induced by the external pump. This active part

$$\varepsilon_g(\mathbf{x}, \{k_{\nu}, \Psi_{\nu}\}) = \frac{\gamma_{\perp}}{k_{\mu} - k_a + i\gamma_{\perp}} \frac{D_0(\mathbf{x}, d)}{1 + \sum_{\nu} \Gamma_{\nu} |\Psi_{\nu}|^2}, \quad (2)$$

contains modal interactions and gain saturation, due to spatial hole burning through the nonlinearity given by  $[1 + \sum_{\nu} \Gamma_{\nu} |\Psi_{\nu}|^2]^{-1}$ , where  $\Gamma_{\nu} = \Gamma(k_{\nu})$  is a Lorentzian

function of width  $2\gamma_{\perp}$ , centered at the atomic transition frequency  $k_a$  and evaluated at the lasing frequency  $k_{\mu}$  ( $c = 1$ ). Crucially,  $\varepsilon_g$  in Eq. (2) also contains the spatially varying inversion density  $D_0(\mathbf{x}, d)$ , the “pump” [26], where we have introduced an adiabatic parameter  $d$ . This leads us to the concept of a “pump trajectory” (see, e.g., Fig. 1) consisting of a sequence of adiabatic variations in both the pump profile and amplitude, parametrized by  $d$  and satisfying  $\frac{dD_0}{dt} \ll \gamma_{\parallel}$  to ensure adiabaticity ( $\gamma_{\parallel}$  is the longitudinal relaxation rate) [20, 25]. We obtain the solutions to Eq. (1) along such a pump trajectory for both the laser frequency  $k_{\mu}$  and the corresponding electric field  $\Psi_{\mu}$  as the fixed points of a self-consistent iteration carried out for each given value of the pump  $D_0(\mathbf{x}, d)$  [27]. With this procedure, we find the full *nonlinear* solutions for the emission intensities above threshold; as we now demonstrate, the qualitative behavior shown in Fig. 1 is, however, determined already by the *linear* threshold conditions for a given pump trajectory.

To show this, we introduce a generalization of the threshold equations of SALT, which are posed in two steps. First we define a non-Hermitian eigenvalue problem,

$$\left[ \nabla^2 + k^2 \left( \varepsilon_c(k) + \eta_n(k, d) D_0(\mathbf{x}, d) \right) \right] u_n(k, d; \mathbf{x}) = 0, \quad (3)$$

where  $\eta_n(k, d)$  is the complex eigenvalue [22, 27], and  $\eta_n(k, d) D_0(\mathbf{x}, d)$  plays the role of  $\varepsilon_g$  in Eq. (2) at threshold, where the nonlinearity vanishes. Equation (3), which is solved using non-Hermitian “constant flux” boundary conditions at the laser boundary ( $\partial_x u_n = \pm i k u_n$ ), is a generalization of the threshold constant flux (TCF) equation [22] for pump trajectories; the  $\{u_n, \eta_n\}$  are the TCF states and eigenvalues.

The first laser mode is determined out of the countably infinite set of  $\eta_n(k, d)$  as the one which satisfies

$$\eta_n(k_{\mu}, d_{\mu}) = \frac{\gamma_{\perp}}{k_{\mu} - k_a + i\gamma_{\perp}} \quad (4)$$

for the smallest value of  $d_{\mu}$ , which, from Eq. (4), also yields the threshold lasing frequency  $k_{\mu}$ . The lasing mode  $\psi_{\mu}(\mathbf{x})$  at the threshold is then just given by the corresponding eigenstate  $u_n(k_{\mu}, d_{\mu}; \mathbf{x})$ . The linear non-Hermitian TCF equation, Eq. (3), can, however, be solved for arbitrary values of  $k$  and  $d$ . We are thus naturally provided with the two continuous parameters necessary to demonstrate the presence of EPs in the complex spectrum of the TCF operator [8]. This will bring us to the central insight that the TCF operator which determines the lasing thresholds contains the EPs which control the lasing behavior shown in Fig. 1.

To show this explicitly, we rewrite the complex Eq. (4) as two real conditions which neatly separate the role of

the TCF spectrum and the gain curve

$$|\eta_n|^2 + \text{Im}(\eta_n) = 0, \quad \frac{k - k_a}{\gamma_\perp} = \frac{\text{Im}(\eta_n) + 1}{\text{Re}(\eta_n)}. \quad (5)$$

The left equation has not been analyzed in previous work on SALT; it has the remarkable property of being entirely independent of the gain curve parameters  $k_a$  and  $\gamma_\perp$  (which do not appear in the TCF equation). Hence, it defines a threshold boundary in the  $k, d$  plane dividing lasing and nonlasing regions, solely from the values of  $\{\eta_n\}$ . To conveniently capture the entire  $k, d$  landscape of possible lasing solutions, we define a function  $f(k, d) \equiv \min_n [|\eta_n|^2 + \text{Im}(\eta_n)]$ , which has the property that the contour  $f(k, d) = 0$  is the locus of all possible lasing thresholds. The actual lasing thresholds on this contour are then determined by the gain curve parameters in the right-hand condition of Eq. (5). In Fig. 2, we show the relevant regions of  $f(k, d)$  above ( $f < 0$ , green, within black contour) and below ( $f > 0$ , red, outside black contour) threshold, as well as the threshold boundary ( $f = 0$ , black contour). When  $f < 0$ , the TCF equation does not give the lasing solutions and full nonlinear SALT is needed to find the intensity and frequency,

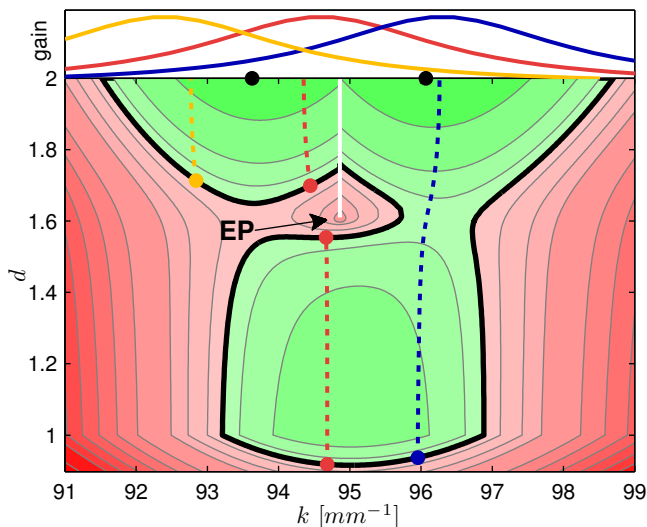


FIG. 2. (color online) Contour plot of the function  $f(k, d)$ , which indicates the parameter regions of  $k$  and  $d$  where the laser in Fig. 1 is above threshold (green, inside black contour) or below threshold (red, outside black contour). The threshold condition,  $f(k, d) = 0$ , is satisfied at the solid black contour. The EP in the center of the plot pulls the laser below the threshold in its vicinity. The frequency dependence of the solutions of the nonlinear SALT equations (dashed lines) and the corresponding laser thresholds (dots on the solid black contour) are provided for the same gain curves (shown in the top panel) as in Fig. 1. The evaluation of  $f(k, d)$  involves two interconnected Riemann sheets (see Fig. 3), resulting in a cut between the two sheets (see the white line right above the EP). The two black dots at the upper edge of the plot represent the resonance frequencies of the passive cavity system.

as was done for the curves in Figs. 1 and 2.

The most striking feature of the contour plot shown in Fig. 2 is the existence of a substantial inclusion of subthreshold region (red, outside black contour) in the midst of the superthreshold region (green, within black contour). At the center of this inclusion is a local maximum of  $f$ ; this point corresponds to an EP of the TCF operator. For the middle gain curve (red), there are three threshold solutions, two very near the EP. If we order these solutions according to increasing pump,  $d$ , we find that  $\partial f / \partial d < 0$  at the first and third thresholds and  $\partial f / \partial d > 0$  at the second. As a function of  $d$ , the laser thus turns on-off-on, just as found in Fig. 1. Hence, nonlinear effects play no role in the qualitative behavior of this laser; they only determine the amplitude of the lasing emission in the green region. All the interesting behavior is controlled by the EP: It completely suppresses lasing in its vicinity of  $k$  and  $d$ -parameters, thereby causing the reentrant lasing (red curve) as well as the nonmonotonic but continuous lasing emission (blue curve), which is influenced by its proximity to the EP.

In the entire  $k$  and  $d$  range shown in Fig. 2, exactly only two eigenvalues  $\eta_{1,2}$  contribute to  $f(k, d)$ . In the coupled cavities studied here, these two eigenvalues are associated with a symmetric-antisymmetric doublet of passive cavity resonances (see black dots in Fig. 2). The doublets are separated from each other by approximately the free spectral range of a single cavity. If both cavities are *uniformly* pumped with the same gain curves as in Fig. 2, the laser emits in modes each of which can be associated with one of the passive resonances (not shown). However, no EP and hence no pump-induced inclusion or nonmonotonic laser emission appears. Only when nonuniform pumping is applied may a pair of eigenvalues coalesce at an EP.

In Fig. 3, we plot the  $k$  and  $d$  dependence of the real and imaginary part of the two eigenvalues  $\eta_{1,2}$ . Focusing on the parameter region around  $d = 1.55$ , where the laser turns off, we find that the parametric dependence of the eigenvalues on  $k$  and  $d$  shows the typical topological

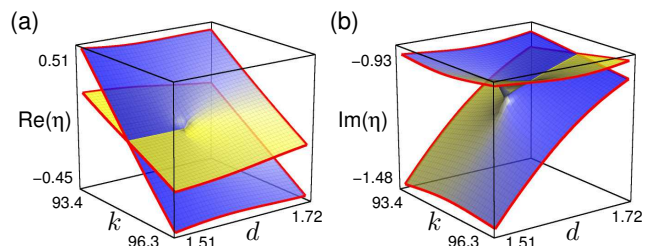


FIG. 3. (color online) (a) Real and (b) imaginary parts of the two eigenvalues  $\eta_{1,2}(k, d)$  which are closest to the threshold in the  $k$  and  $d$  parameter region around the laser turn-off observed in Fig. 1. The eigenvalue surfaces display the typical structure of intersecting Riemann surfaces, centered around an EP.

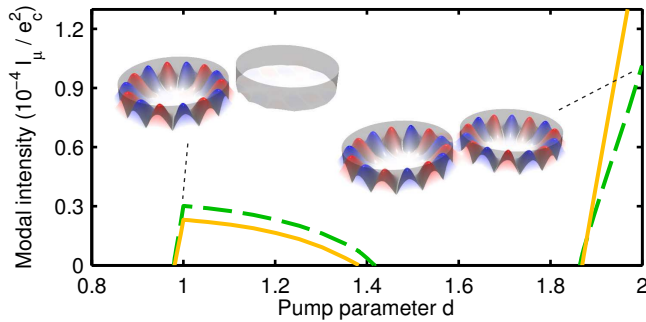


FIG. 4. (color online) Laser light intensity emitted from two coupled microdisks (see insets) as a function of pump parameter  $d$ . With the same pumping scheme as in Fig. 1 (maximum pump in each disk:  $D = 0.71$ ) the laser is also found here to turn off for increasing  $d$ . The disks have a radius of  $45 \mu\text{m}$ , an intercavity spacing of  $10 \mu\text{m}$  and an index of refraction  $n = 3.67 + 0.09i$ . The gain curve parameters are  $k_a \sim 2.82 \text{ THz}$  and  $\gamma_{\perp} \sim 0.29 \text{ THz}$ . The insets show the absolute value of the electric field of the green (dashed) lasing mode at the pump points  $d = 1$  and  $d = 2$ .

structure of two intersecting Riemann sheets around an EP located at  $k \approx 95 \text{ mm}^{-1}$ ,  $d \approx 1.6$ . Away from the EP, the laser can always “choose” the lower threshold solution for lasing (upper part of the Riemann sheet), but at the EP only one solution is available, which is a compromise between the low and high threshold solution. This gives rise to a local minimum in the effective gain and inhibits lasing in the vicinity of the EP. In this way, the essential physics of an EP directly translates into the physical effects observed in Fig. 1.

To confirm that such a behavior is generic for coupled microlasers, we consider a device consisting of two coupled circular microdisks [28, 29] which has recently been implemented as an electrically controllable “photonic-molecule laser” [30]. For this more challenging computation, we have incorporated in the SALT an advanced higher-order finite element method discretization technique [31]. When applying the same pumping scheme as in Fig. 1 to such a coupled microdisk laser (see insets of Fig. 4), we again find that the laser may turn off when increasing the overall pump power (see main panel of Fig. 4). Note, however, that more than one mode is lasing both below and above the turn-off due to a quasidegeneracy of modes. This example demonstrates that the effect of EPs on the above-threshold characteristics of a laser should be generally observable in coupled microlasers.

The success of a corresponding experiment hinges on striking the right balance between the coupling strength and the amount of gain or loss in each disk. Gain or loss is fixed by the cavity material as well as by the applied pumping strength. Microlasers built from active quantum cascade structures (QCLs) seem to be ideally suited to test this effect, since they can be well-controlled in

their shape and hence in their coupling. With the active medium being situated within a lossy metal waveguide [32], a central requirement for observing this effect, i.e., that the absorption length in the passive cavity is smaller than the round trip length, has already been experimentally realized for a variant of such lasers [33]. Also, a sufficiently strong inter-cavity coupling has been demonstrated for such coupled QCLs [30, 33], suggesting that an experimental realization might be within reach. Note that we have used realistic material parameters from the experiment [30] in the employed MB equations which typically describe QCLs very well [34].

To summarize, we have shown that the presence of an exceptional point in the lasing equations for coupled microlasers may be “brought to light” by a suitable variation of the applied pumping. We find that, in the vicinity of the exceptional point, the output intensity of the emitted laser light is *reduced*, although the applied pump power is *increased*. This unorthodox and robust lasing effect may even turn off a laser above its lowest threshold. We suggest an experimental realization of this effect, which would open up many more possibilities to study the rich physics associated with EPs in the pump dependence of a laser.

The authors would like to thank the following colleagues for very fruitful discussions: A. Benz, M. Brandstetter, C. Deutsch, S. Esterhazy, G. Fasching, T. Führer, M. Janits, K. G. Makris, M. Martl, J. M. Melenk, H. Ritsch, J. Schöberl, K. Unterrainer and J. Vilsecker. Financial support by the Vienna Science and Technology Fund (WWTF) through project MA09-030 and by the Austrian Science Fund (FWF) through Project No. SFB IR-ON F25-14 as well as computational resources by the Vienna Scientific Cluster (VSC) and the Yale High Performance Computing Cluster (Yale HPC) are gratefully acknowledged. H.E.T. acknowledges support from the Swiss NSF Grant No. PP00P2-123519/1, NSF Grant No. EEC-0540832 (MIRTHE), and DARPA Grant No. N66001-11-1-4162 and A.D.S. from NSF Grant No. DMR-0908437.

\* [matthias.liertzer@tuwien.ac.at](mailto:matthias.liertzer@tuwien.ac.at)

† [stefan.rotter@tuwien.ac.at](mailto:stefan.rotter@tuwien.ac.at)

- [1] A. Guo, G. J. Salamo, D. Duchesne, R. Morandotti, M. Volatier-Ravat, V. Aimez, G. A. Siviloglou, and D. N. Christodoulides, *Phys. Rev. Lett.* **103**, 093902 (2009).
- [2] C. E. Rüter, K. G. Makris, R. El-Ganainy, D. N. Christodoulides, M. Segev, and D. Kip, *Nat. Phys.* **6**, 192 (2010).
- [3] W. Wan, Y. Chong, L. Ge, H. Noh, A. D. Stone, and H. Cao, *Science* **331**, 889 (2011).
- [4] B. Dietz, H. L. Harney, O. N. Kirillov, M. Miski-Oglu, A. Richter, and F. Schäfer, *Phys. Rev. Lett.* **106**, 150403 (2011).
- [5] S. B. Lee, J. Yang, S. Moon, S. Y. Lee, J. B.



- Shim, S. W. Kim, J. H. Lee, and K. An, *Phys. Rev. Lett.* **103**, 134101 (2009).
- [6] Y. Choi, S. Kang, S. Lim, W. Kim, J. R. Kim, J. H. Lee, and K. An, *Phys. Rev. Lett.* **104**, 153601 (2010).
- [7] J. Schindler, A. Li, M. C. Zheng, F. M. Ellis, and T. Kottos, *Phys. Rev. A* **84**, 040101 (2011).
- [8] W. D. Heiss, *J. Phys. A* **37**, 2455 (2004).
- [9] J. W. Ryu, S. Y. Lee, and S. W. Kim, *Phys. Rev. A* **79**, 053858 (2009).
- [10] J. Wiersig, A. Eberspacher, J. B. Shim, J. W. Ryu, S. Shinohara, M. Hentschel, and H. Schomerus, *Phys. Rev. A* **84**, 023845 (2011).
- [11] R. Lefebvre, O. Atabek, M. Šindelka, and N. Moiseyev, *Phys. Rev. Lett.* **103**, 123003 (2009).
- [12] C. M. Bender and S. Boettcher, *Phys. Rev. Lett.* **80**, 5243 (1998).
- [13] Y. D. Chong, L. Ge, and A. D. Stone, *Phys. Rev. Lett.* **106**, 093902 (2011).
- [14] K. G. Makris, R. El-Ganainy, D. N. Christodoulides, and Z. H. Musslimani, *Phys. Rev. Lett.* **100**, 103904 (2008).
- [15] S. Klaiman, U. Günther, and N. Moiseyev, *Phys. Rev. Lett.* **101**, 080402 (2008).
- [16] H. Schomerus, *Phys. Rev. Lett.* **104**, 233601 (2010).
- [17] S. Longhi, *Phys. Rev. A* **82**, 031801 (2010).
- [18] L. Ge, Y. D. Chong, S. Rotter, H. E. Türeci, and A. D. Stone, *Phys. Rev. A* **84**, 023820 (2011).
- [19] When Figs. 1 and 2 are printed in grayscale, note that yellow corresponds to light gray, red to gray, and blue to dark gray..
- [20] H. Haken, *LIGHT II - Laser Light Dynamics*, 1st ed. (North Holland, 1985).
- [21] M. Sargent, M. O. Scully, and W. E. Lamb, *Laser physics* (Perseus Books, 1977).
- [22] L. Ge, Y. D. Chong, and A. D. Stone, *Phys. Rev. A* **82**, 063824 (2010).
- [23] H. E. Türeci, A. D. Stone, L. Ge, S. Rotter, and R. J. Tandy, *Nonlinearity* **22**, C1 (2009).
- [24] H. E. Türeci, A. D. Stone, and B. Collier, *Phys. Rev. A* **74**, 043822 (2006).
- [25] L. Ge, R. J. Tandy, A. D. Stone, and H. E. Türeci, *Opt. Express* **16**, 16895 (2008).
- [26] Both the scalar mode  $\Psi_\mu$ , the real part of which corresponds to the electric field, and the pump  $D_0$  are given here in their natural units  $e_c$  and  $d_c$  [22].
- [27] M. Liertzer, *Nonlinear interactions in coupled micro-lasers*, Master's thesis, University of Technology Vienna (2011).
- [28] S. Preu, H. G. L. Schwefel, S. Malzer, G. H. Döhler, L. J. Wang, M. Hanson, J. D. Zimmerman, and A. C. Gossard, *Opt. Express* **16**, 7336 (2008).
- [29] H. Ramezani, T. Kottos, V. Shuvayev, and L. Deych, *Phys. Rev. A* **83**, 053839 (2011).
- [30] G. Fasching, C. Deutsch, A. Benz, A. M. Andrews, P. Klang, R. Zobl, W. Schrenk, G. Strasser, P. Ragulis, V. Tamošiūnas, and K. Unterrainer, *Opt. Express* **17**, 20321 (2009).
- [31] We employ the open source finite element mesher netgen (J. Schöberl, *Computing and Visualization in Science* **1**, 41 (1997)) and the corresponding solver NGSolve available from <http://sf.net/projects/ngsolve>
- [32] M. Martl, J. Darmo, C. Deutsch, M. Brandstetter, A. M. Andrews, P. Klang, G. Strasser, and K. Unterrainer, *Opt. Express* **19**, 733 (2011).
- [33] C. Schwarzer, E. Mujagić, Y. Yao, W. Schrenk, J. Chen, C. Gmachl, and G. Strasser, *Appl. Phys. Lett.* **97**, 071103 (2010); E. Mujagić, S. Schartner, L. K. Hoffmann, W. Schrenk, M. P. Semtsiv, M. Wienold, W. T. Masselink, and G. Strasser, *Appl. Phys. Lett.* **93**, 011108 (2008).
- [34] A. K. Wójcik, N. Yu, F. Capasso, and A. Belyanin, *J. Mod. Opt.* **58**, 727 (2011).